



Regulatory Dynamics of Cell Differentiation Revealed by True Time Series From Multinucleate Single Cells

Anna Pretschner¹, Sophie Pabel¹, Markus Haas¹, Monika Heiner² and Wolfgang Marwan^{1*}

¹ Magdeburg Centre for Systems Biology and Institute of Biology, Otto von Guericke University, Magdeburg, Germany,

² Computer Science Institute, Brandenburg University of Technology Cottbus-Senftenberg, Cottbus, Germany

OPEN ACCESS

Edited by:

Jianhua Xing,
University of Pittsburgh, United States

Reviewed by:

Shou-Wen Wang,
Harvard Medical School,
United States
Junyue Cao,
The Rockefeller University,
United States

*Correspondence:

Wolfgang Marwan
wolfgang.marwan@ovgu.de

Specialty section:

This article was submitted to
Systems Biology,
a section of the journal
Frontiers in Genetics

Received: 30 September 2020

Accepted: 07 December 2020

Published: 08 January 2021

Citation:

Pretschner A, Pabel S, Haas M,
Heiner M and Marwan W (2021)
Regulatory Dynamics of Cell
Differentiation Revealed by True Time
Series From Multinucleate Single
Cells. *Front. Genet.* 11:612256.
doi: 10.3389/fgene.2020.612256

Dynamics of cell fate decisions are commonly investigated by inferring temporal sequences of gene expression states by assembling snapshots of individual cells where each cell is measured once. Ordering cells according to minimal differences in expression patterns and assuming that differentiation occurs by a sequence of irreversible steps, yields unidirectional, eventually branching Markov chains with a single source node. In an alternative approach, we used multi-nucleate cells to follow gene expression taking true time series. Assembling state machines, each made from single-cell trajectories, gives a network of highly structured Markov chains of states with different source and sink nodes including cycles, revealing essential information on the dynamics of regulatory events. We argue that the obtained networks depict aspects of the Waddington landscape of cell differentiation and characterize them as reachability graphs that provide the basis for the reconstruction of the underlying gene regulatory network.

Keywords: single cell time series, gene regulatory network, Petri net, Markov chain, systems biology, Waddington landscape

INTRODUCTION

Single-cell analyses revealed complex dynamics of gene regulation in differentiating cells (Spiller et al., 2010; Junker and van Oudenaarden, 2014; Paul et al., 2015; Marr et al., 2016; Plass et al., 2018). It is believed that dynamic effects possibly superimposed by stochastic fluctuations in gene expression levels may play crucial roles in cell fate choice, commitment, and reprogramming (Graf and Enver, 2009; Huang et al., 2009; Zhou and Huang, 2011; Ferrell Jr., 2012; Il Joo et al., 2018; Bornholdt and Kauffman, 2019). Changes in gene expression over time have not been directly measured in single mammalian cells as cells are - for technical reasons - sacrificed during the analysis procedure and hence can be measured only once. Instead, algorithms have been developed to infer the gene expression trajectory of a typical cell in pseudo-time from static snapshots of gene expression states in a cell population, resulting in Markov chains of states (Bendall et al., 2014; Cannoodt et al., 2016; Chen et al., 2019; Saelens et al., 2019; Setty et al., 2019). Most trajectory inference algorithms are based on the assumption that differentiation is unidirectional (Bendall et al., 2014; Haghverdi et al., 2016; Street et al., 2018; Saelens et al., 2019) and that the probability of transiting from one state to the next similar state is independent of the individual history of

a cell (Setty et al., 2019). The inference of trajectories has been used to create pseudo-time series for differentiation (Marco et al., 2014; Moignard et al., 2015; Shin et al., 2015; Macaulay et al., 2016), cell cycle (Kafri et al., 2013), and the response to perturbation (Gaublomme Jellert et al., 2015). As any given distribution of expression patterns could result from multiple dynamics, the reconstruction of trajectories from snapshots faces fundamental limits (Weinreb et al., 2018). Even though regulatory mechanisms cannot be directly and rigorously inferred from snapshots (Weinreb et al., 2018), dynamic analyses may be of immediate importance to resolve competing views on basic mechanisms and the role of stochasticity in cell fate decisions (Moris et al., 2016).

True single cell time series can be obtained in *Physarum polycephalum* by taking multiple samples of one and the same giant cell. *Physarum* belongs to the amoebozoa group of organisms. It has a complex, prototypical eukaryote genome (Schaap et al., 2016) and forms different cell types during its life cycle (Alexopoulos and Mims, 1979).

Giant, multi-nucleate cells, so-called plasmodia provide a source of macroscopic amounts of homogeneous protoplasm with a naturally synchronous population of nuclei, which is continually mixed by vigorous shuttle-streaming (Guttes and Guttes, 1961, 1964; Rusch et al., 1966; Dove et al., 1986). The differentiation of a plasmodium into fruiting bodies involves extensive remodeling of signal transduction and transcription factor networks with alterations at the transcriptional, translational, and post-translational level (Glöckner and Marwan, 2017).

In starving plasmodial cells, the formation of fruiting bodies can be experimentally triggered by a brief pulse of far-red light received by phytochrome as photoreceptor (Starostzik and Marwan, 1995b; Lamparter and Marwan, 2001; Schaap et al., 2016). Retrieving small samples of the same plasmodial cell before and at different time points after an inductive light pulse allows to follow how gene expression changes over real time. Because cell cycle, cell fate choice, and development are synchronous throughout the plasmodium (Rusch et al., 1966; Starostzik and Marwan, 1995a; Hoffmann et al., 2012; Walter et al., 2013; Rätzel and Marwan, 2015), single-cell gene expression trajectories can indeed be constructed from time series. By assembling finite state machines made from trajectories we have constructed Petri net models for the state transitions that predict Markov chains as variable developmental routes to differentiation (Werthmann and Marwan, 2017; Rätzel et al., 2020) which may be considered as trajectories through the Waddington landscape (Waddington, 1957; Huang et al., 2009). These Petri nets also predict reversible and irreversible steps, commitment points, and meta-stable states in cells responding to a differentiation stimulus. However, the computational approach for the construction of Petri nets from time series has been originally developed with data sets of a coarse resolution in time and the structural resolution of the nets was accordingly limited. Nevertheless, the approach turned out to be useful for capturing the dynamics of the process. For this paper, we developed a method for retrieving smaller samples from even larger plasmodial cells and showed that these cells provide a homogeneous source for samples to

be taken. This allowed us to considerably improve the time resolution as compared to previous studies. Sampling cells at higher time resolution, allowed the construction of Petri nets with enhanced structural and dynamic resolution. Structural complexity, highly connected nodes, parallel pathways, reversible reactions, and Petri net places representing meta-stable states in the developmental network, as revealed by the new data sets, characterize the differentiation response as complex and dynamic in contrast to a smooth, continuous process. We describe the graph properties of the Waddington Petri nets and conclude that the gene expression dynamics revealed by our analysis most likely emerge from the non-linear dynamic behavior of the underlying regulatory network rather than from stochastic fluctuations in the concentration of regulatory molecules.

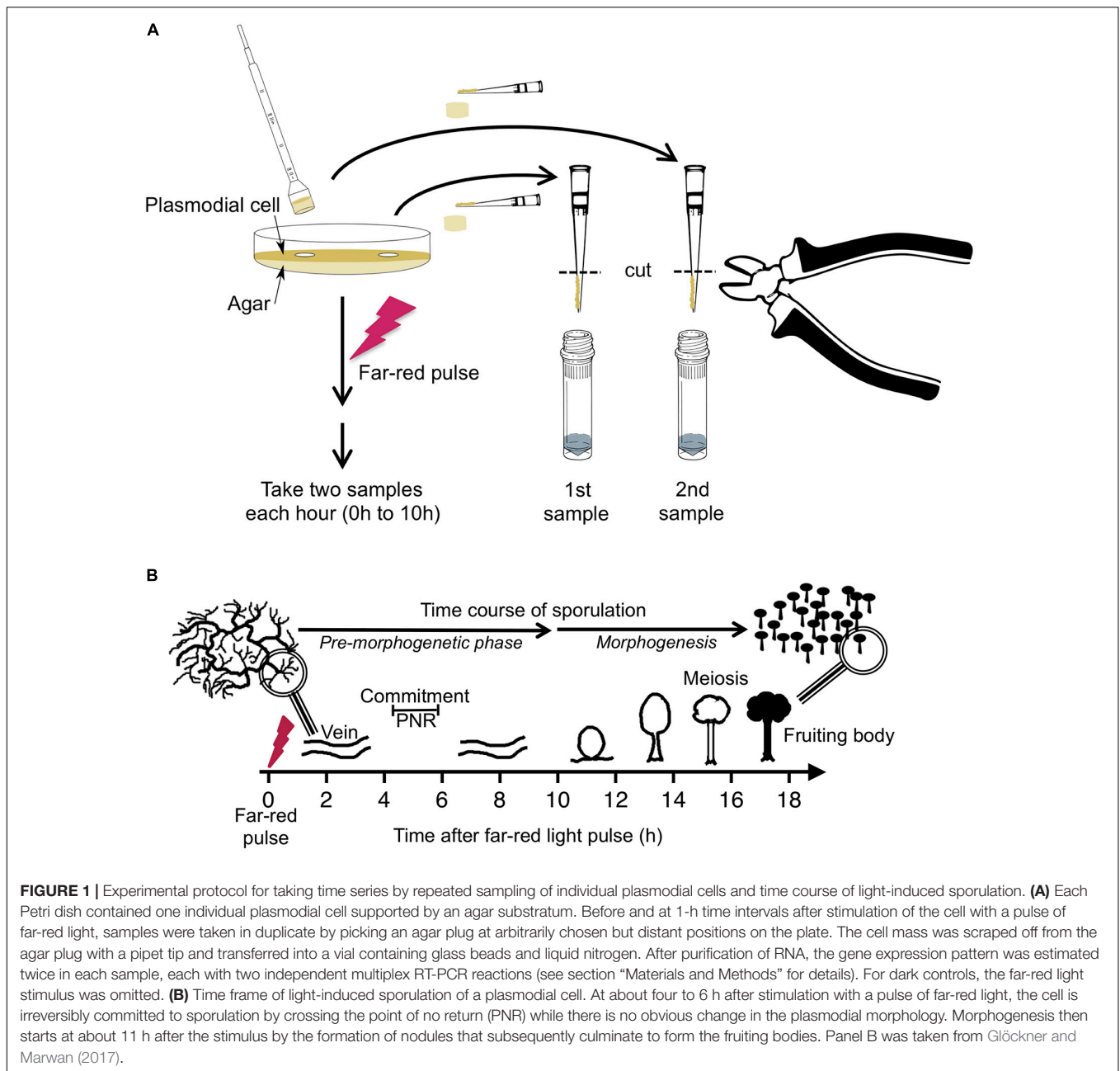
MATERIALS AND METHODS

Plasmodial Strain, Growth of Cells, Sample Preparation, and Gene Expression Analysis

Sporulation-competent plasmodial cells of wild type strain LU897 × LU898 (Starostzik and Marwan, 1998) were obtained as previously described (Starostzik and Marwan, 1998; Rätzel et al., 2020). A total of 2.8 gram of plasmodial mass was applied to a 14 cm Ø Petri dish that contained 90 ml of semi-rich Golderer agar (Golderer et al., 2001), based on a salt solution of 0.01% (w/v) niacin, 0.01% (w/v) niacinamide, 0.1% (w/v) CaCO₃, and 0.14 mM CuCl₂, supplemented with 5 g peptone from meat (Sigma Aldrich), 0.75 g yeast extract (Becton, Dickinson & Co.), and 3.9 mM glucose per liter, adjusted to pH 4.6 with concentrated HCl. After starvation for 7 days at 22°C in complete darkness, sporulation was induced with a 15 min pulse of far-red light ($\lambda \geq 700$ nm, 13 W/m²) (Starostzik and Marwan, 1998). Before and at 1-h time intervals after the start of the far-red pulse, samples were taken in duplicate at arbitrarily chosen but distant positions on the plate. Each sample was obtained by picking an agar plug of 1.13 cm² with the cut bulb of a disposable Pasteur pipette (EA62.1; Carl Roth, Karlsruhe, Germany). The plasmodial mass on the agar plug was scraped off with a pipet tip and, by cutting the tip, transferred into a vial of glass beads immersed in liquid nitrogen (**Figure 1**). After extraction of RNA and removal of contaminating DNA (Marquardt et al., 2017), the relative abundance of the mRNAs of 35 genes, differentiation marker and reference genes (Hoffmann et al., 2012; **Supplementary Table 2**) was analyzed by gene expression profiling (GeXP), a multiplex RT-PCR method (Hayashi et al., 2007) as previously described (Rätzel and Marwan, 2015; Marquardt et al., 2017).

Data Analysis Pipeline and Automated Generation of Petri Nets

To correct for differences in the concentration of total RNA and in the efficiency of the RT-PCR reaction, the gene expression values were normalized to the median of the estimated relative concentrations of mRNAs of the 35 genes in each RNA sample. Each normalized expression value was subsequently normalized



to the geometric mean of all values obtained for a given gene, and this was performed separately for each gene.

Data were analyzed and processed with a revised and extended pipeline written in R (R Core Team., 2016), based on the previously described script (Rätzel et al., 2020). The normalized gene expression data were clustered and significant clusters were determined with the help of the Simprof algorithm (Clarke et al., 2008) as provided by the clustsig package (Whitaker and Christman, 2014). Expression patterns were visualized in the form of a heatmap generated by the heatmap.2 function, provided as part of the gplots package (Warnes et al., 2016). Changes in gene expression over time were visualized by multidimensional

scaling based on Euclidean distance (Gower, 1966) with the help of the *cmdscale* function provided as part of the stats package v3.5.1 (R Core Team., 2016). Petri nets were constructed from single cell trajectories of gene expression as previously described (Rätzel et al., 2020). Each trajectory is a temporal sequence of gene expression states, where each state corresponds to a Simprof significant cluster. Petri nets specified in ANDL format (Abstract Net Description Language) (Heiner et al., 2013) were imported into Snoopy (Rohr et al., 2010) and graphically displayed by running the Sugiyama layout algorithm (Sugiyama et al., 1981). Petri net places, each representing a gene expression state, were colored according to the relative temporal stability

of the expression state or according to the relative frequency with which each gene expression state occurred. Petri net transitions, corresponding to transits between states were colored according to the frequency with which each transit occurred or according to the data subset in which the transit occurred. These parameters were computed and coloring was performed by automatic editing of Snoopy files encoded in xml format, again with the help of a R script. The raw data and the complete computational pipeline used in this study is provided as part of the **Supplementary Material**.

RESULTS

Even Large Plasmodia Provide a Source of Homogeneous Cell Material for True Time Series Analysis of Gene Expression

In previous studies we have shown that the gene expression pattern in samples taken at the same time from different sites of a plasmodium covering a standard Petri dish (9 cm Ø) did not change within the limits of accuracy of the measurements. Accordingly, repeated sampling of the same plasmodial cell yields true time series (Rätzel, 2015; Werthmann and Marwan, 2017). To allow more samples to be taken without consuming too much of the plasmodial mass, we now prepared plasmodia on 14 cm Ø Petri dishes, increasing the surface area covered by the plasmodial mass by 2.4-fold, and took smaller samples by punching agar plugs of 1.13 cm² per sample, to harvest a small portion of the initial total plasmodial mass. To test whether the homogeneity in gene expression is impaired or even lost in the larger plasmodia, we took 9 or 16 samples at the same time from approximately evenly spread sites of a plasmodium, and estimated the gene expression pattern twice in the RNA of each sample, to obtain one technical replicate of each measurement (Aselmeyer, 2019; Driesch, 2019). This allowed to estimate the biological variation in gene expression within a plasmodium as compared to the technical accuracy of the measurements. In order to correct for potential differences in the efficiency of the RT-PCR between reactions, the expression value for each gene was normalized to the median of the expression values of all genes measured in the sample (for details see Materials and Methods). To estimate the technical accuracy of the measurements, the relative deviation of first and second measurement from the mean of the two measurements was estimated for each assayed gene in each of the retrieved plasmodial samples. The frequency distribution of all values was almost symmetrical with a tail consisting of a small number of low values, obviously as a result of inefficient RT-PCR reactions. To estimate the degree of homogeneity in gene expression within a plasmodial cell, we asked to which extent the expression values for the 9 or 16 samples taken from the same plasmodium deviated from their median. To restrict the influence of technical artifacts on the result, we considered the subset of the data where first and the second measurement of the same plasmodial sample deviated not more than two-fold from the mean of the two values. In three of the total of 46 analyzed plasmodia (30 far-red stimulated; 16 dark controls), individual

samples deviated from the rest of the samples of the same plasmodium by more than a factor of two. As errors in sample preparation could not be ruled out, these three plasmodia were excluded and the remaining data set of 43 plasmodia (28 far-red stimulated; 15 dark controls) was analyzed taking the mean of 1st and 2nd measurement for each gene in each sample. Among the total of 7160 values, 98% of the symmetric frequency distribution (**Supplementary Figure 1**) were between 0.48- and 2.10-fold deviation of the median of all values of the respective plasmodium (**Supplementary Table 1**). There was no obvious difference between dark controls and far-red stimulated plasmodia which were measured at 6 h after the light pulse when genes were already differentially regulated (**Supplementary Figure 1** and **Supplementary Table 1**), indicating that even during the period where the mRNA abundance changed in time, the homogeneity in gene expression levels is maintained. Visual inspection of outliers within the distribution did not reveal any candidates for specific genes that might be inhomogeneously expressed.

In summary, the gene expression values throughout a plasmodium deviated not more than approximately two-fold from the median of all samples from the same plasmodium and were thus within the limits of the technical accuracy of the measurements, even under conditions where genes were in the process of being up- or down-regulated. These differences measured between samples were minor as compared to the differential regulation where the expression level of genes changed in the order of ten to more than hundred-fold (**Supplementary Figure 2**). These results are consistent with the results of the time-series experiment, where for each time point, two samples were retrieved and analyzed from the same plasmodial cell (see below).

Sampling of Plasmodia at 1 h Time Interval

As the assayed genes were evenly expressed and changed evenly in time throughout the large plasmodia, at least within the limits of accuracy of the measurements, we took time series at 1 h time intervals. In order to assay, in each experiment, for the homogeneity and synchrony in gene expression throughout the plasmodium, we took two samples at each time point from different, arbitrarily chosen but distant sites of the plasmodium (**Figure 1**). In far-red stimulated plasmodia, the first samples (referred to as the 0 h samples) were taken at the start of the experiment, i.e., immediately before application of the 15 min pulse of far-red light. All subsequent samples were taken at 1 h time intervals until 10 h after the start of the experiment [At 5 to 6 h after the far-red pulse cells have passed the commitment point, while visible morphogenesis starts several hours later by entering the transient nodulation stage at about 11 h after the pulse (Hoffmann et al., 2012)]. In the dark controls, the far-red stimulus was omitted. Gene expression in each plasmodial sample taken at a given time point was analyzed twice by GeXP-RT-PCR, where the measurement and the corresponding technical replicate are referred to as 1st and 2nd measurement for sample #1, and 3rd and 4th measurement for sample #2, respectively. Data were normalized as described above.

The technical quality of the measurements was estimated separately for the two data sets, each comprising the data of the samples collected at the 11 time points of the time series. For each plasmodial sample, the relative deviation of the two measurements (1st and 2nd, or 3rd and 4th) from the mean of the two measurements was estimated. The frequency distributions of the deviations and corresponding quantil values indicated that the technical qualities of 1st and 2nd, as well as 3rd and 4th measurement were virtually identical with 95% of the values differing less than a factor of two from each other (**Figure 2** and **Table 1**).

The degree of spatial variability of gene expression within a plasmodium was estimated by combining the data sets for the first and the second sample of a plasmodium taken at each time point of the time series. The frequency distribution of the deviation of each measurement from the mean of 1st, 2nd, 3rd, and 4th measurement of the two samples taken from each plasmodium at any time point was virtually identical to the frequency distributions obtained for the technical replicates, indicating that gene expression within the analyzed plasmodia varied at maximum within the limits of accuracy of the measurements (within a factor of 2 in 95% of the samples). This conclusion is based on the comparison of the quantile distributions of the data sets (**Figure 2** and **Table 1**) considering a total of 36,540 data points.

Multi-Dimensional Scaling Analysis

With this data set, we investigated how expression changes as a function of time in the individual plasmodial cells. The gene expression pattern of a plasmodial cell at a given time point was obtained as the mean of the four expression values of each gene measured in the two plasmodial samples picked at that time point.

For visual representation of the data set and of single-cell trajectories of gene expression, we performed multidimensional scaling (MDS) to obtain a data point for the expression pattern of each cell at each time point. Single-cell trajectories of gene expression are shown in **Figure 3**. Notably, the gene expression patterns of un-stimulated cells (dark controls) changed as a function of time with the highest variability along coordinate 2 of the MDS plot **Figures 3A,B**. Trajectories of far-red stimulated cells (**Figures 3C,D**) moved from the left side to the right side of the plot, while the shape of individual trajectories varied to a certain extent, indicating that the response of the cells was similar though not identical. Obviously, the trajectories of six of the eight far-red-stimulated plasmodia of experiment #1 traversed a considerably larger area of the MDS plot (**Figure 3C**) as compared to the other stimulated cells, indicating a larger variation in gene expression during the response to the stimulus. The extent of variation is accordingly obvious when the bulk of data points is placed in the same plot (**Figure 4A**). To search for genes that may account for the scattering along coordinate 2, we visually inspected the individual time series displayed in the form of a heat map (**Supplementary Figure 2**). In addition to the genes that were clearly up- or down-regulated in response to the stimulus, the messages of four genes, *hstA*, *nhpA*, *pcnA*, and *uchA*,

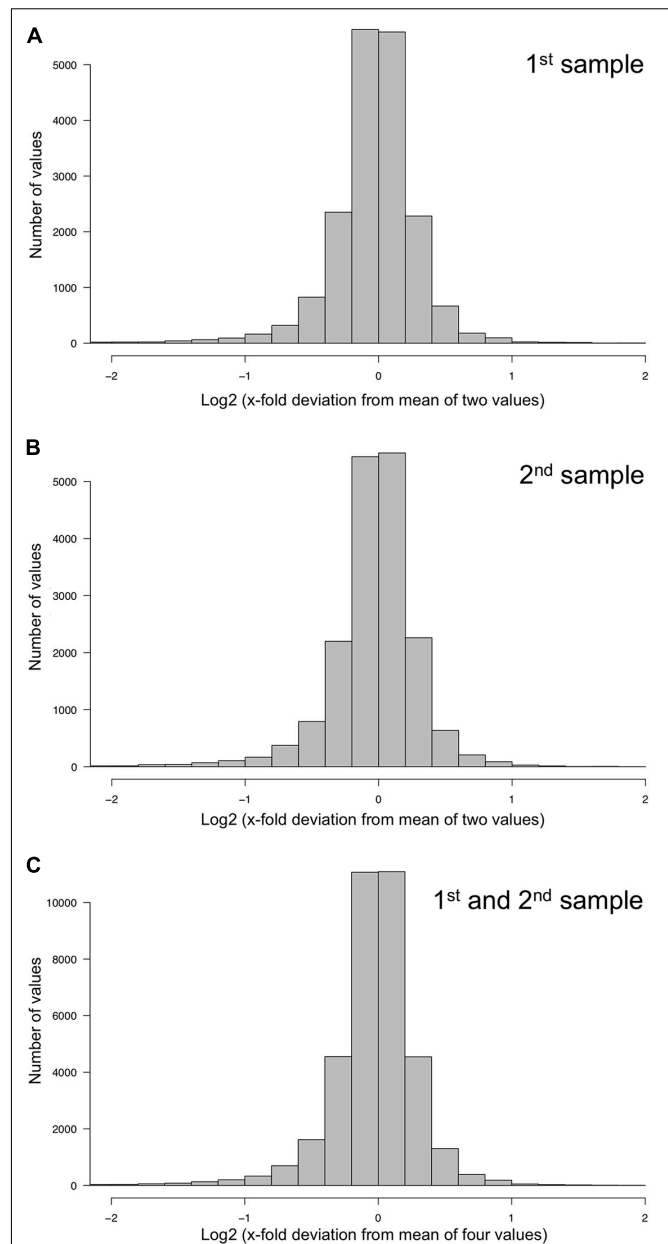


FIGURE 2 | Technical accuracy of measurements and homogeneity of gene expression within a plasmodial cell as determined by technical and biological replicates, taken in experiments #1 and #2 (**Table 2**). **(A,B)** Technical accuracy of measurements of gene expression. The concentration of the mRNAs of the set of 35 genes (**Supplementary Table 2**) was determined twice by RT-PCR for each RNA sample. The frequency distributions display the Log₂ of the x-fold deviation of each expression value of each gene from the mean of the two values obtained by technical replication. Panels **(A,B)** show the results obtained for each of the two biological samples [(**A**), sample #1; (**B**), sample #2], that both were simultaneously taken from the same plasmodial cell at any time point during the experiments. **(C)** Combination of the data sets shown in panels **(A,B)**. This frequency distribution shows the deviation of each measurement from the mean of four values, obtained by twice measuring each of the two biological samples simultaneously taken from the same plasmodium at any time point of the experiments. The figure represents the complete data set of 36,540 data points that was analyzed in the present study.

TABLE 1 | Quantil distributions of the x-fold deviation (x) of a value from the mean of two or four values, characterizing the reproducibility of measurements as estimated through technical and biological replicates, respectively.

Measurements	1st and 2nd		3rd and 4th		1st to 4th	
	Quantile (Log2 (x))	Quantile (x)	Quantile (Log2 (x))	Quantile (x)	Quantile (Log2 (x))	Quantile (x)
1%	-1.308	0.404	-1.383	0.383	-1.349	0.392
5%	-0.555	0.681	-0.592	0.663	-0.574	0.672
25%	-0.169	0.890	-0.169	0.890	-0.169	0.890
50%	-0.010	0.993	-0.008	0.995	-0.009	0.994
75%	0.137	1.100	0.142	1.103	0.139	1.101
95%	0.414	1.333	0.415	1.334	0.415	1.333
99%	0.750	1.682	0.746	1.677	0.747	1.679

The table quantitatively characterizes the frequency distributions shown in **Figure 2**.

in the following called *pcnA*-group genes, changed over time in some of the plasmodia, but there was no obvious consistent relationship to the time point of stimulus application. When only genes were included in the analysis that were clearly up- or down-regulated in response to the stimulus (**Supplementary Figure 2**, see also **Figure 8**), the data points of the MDS plot were indeed less scattered (**Figure 4B**). A qualitatively similar result was obtained plotting the up-regulated and the down-regulated genes separately (**Figures 4C,D**), with some more variation in the expression of the down-regulated genes. However, expression of the *pcnA*-group over time (**Figure 4E**) was clearly different from the up- or down-regulated genes. Expression of the *pcnA*-group genes was different between cells from experiments #1 and #2 as seen from the trajectories of the cells (**Supplementary Figure 3**), suggesting that ongoing internal processes in cells of experiment #1 might even influence their response to the light stimulus. Indeed, according to the corresponding MDS plots of the bulk data points (**Supplementary Figure 4**) the response of the up- and down-regulated genes was less uniformly in cells of experiment #1 (**Supplementary Figure 4C**) as compared to those of experiment #2 (**Supplementary Figure 4D**).

Construction and Graph Properties of Waddington Landscape Petri Nets

For a further analysis, we performed hierarchical clustering of the expression data for all assayed 35 genes, differentiation marker and reference genes (**Supplementary Table 2**), and identified significantly different clusters of expression patterns with the help of the Simprof algorithm (Clarke et al., 2008; **Supplementary Figure 5**). The temporal sequences of gene expression patterns classified as Simprof significant clusters defined a trajectory for each individual cell and revealed significant differences between cell trajectories (**Table 2**). To relate gene expression states and trajectories we constructed a Petri net (bipartite graph) as previously described (Werthmann and Marwan, 2017; Rätzel et al., 2020), by representing each gene expression state by a *place* and the temporal transit between two states by a *transition* (**Figure 5**). A single token marking one place of the Petri net indicates the current gene expression state of a cell. The token moves from its place to a downstream place when the transition, connecting the two places through directed arcs, fires. As each

transition is connected to exactly two places (one pre-place and one post-place), tokens are neither formed nor destroyed when moving through the net, so the gene expression state of the cell remains unequivocally defined at any time. The coherent Petri net obtained this way represents a state machine predicting possible developmental trajectories in terms of Markov chains of gene expression states (Rätzel et al., 2020).

The basic modeling principles are summarized in **Table 3**. We observe the following structural properties of the model which we call ‘*Waddington landscape Petri net*’:

- Each transition has exactly one pre-place and one post-place.
- There are places having more than one post-transition. These post-transitions are in conflict. But, because every transition has exactly one preplace, each conflict is a free choice conflict, meaning the token is free to choose which route to take, predicting a corresponding free choice for the cell (see Discussion).
- There are places having more than one pre-transition, i.e., alternative paths may re-join. Thus, the Petri net structure does not form a tree.
- There are cycles: a cell may switch back to previous states or oscillate between states as defined by the expression patterns of the set of observed genes.

For technical reasons we add immediate transitions starting alternative trajectories, in order to get a statistical distribution of states in which the experiments have started or will start with a given probability.

In contrast to most state-of-the-art pseudo-time series approaches found in the literature (Saelens et al., 2019), the structure of the Waddington landscape Petri net is not restricted to a partial order, meaning it is neither restricted to a directed acyclic graph nor to a tree. Instead we obtain what is known in Petri net theory as ‘*state machine*,’ also called in other communities ‘*finite state machine*’ or ‘*finite automata*,’ which may involve cycles.

A state machine with one token and its reachability graph, or Markov chain for stochastic Petri nets, are isomorph (i.e., have the same structure, there is a 1-to-1 correspondence); to put it differently: our (stochastic) Petri net represents the

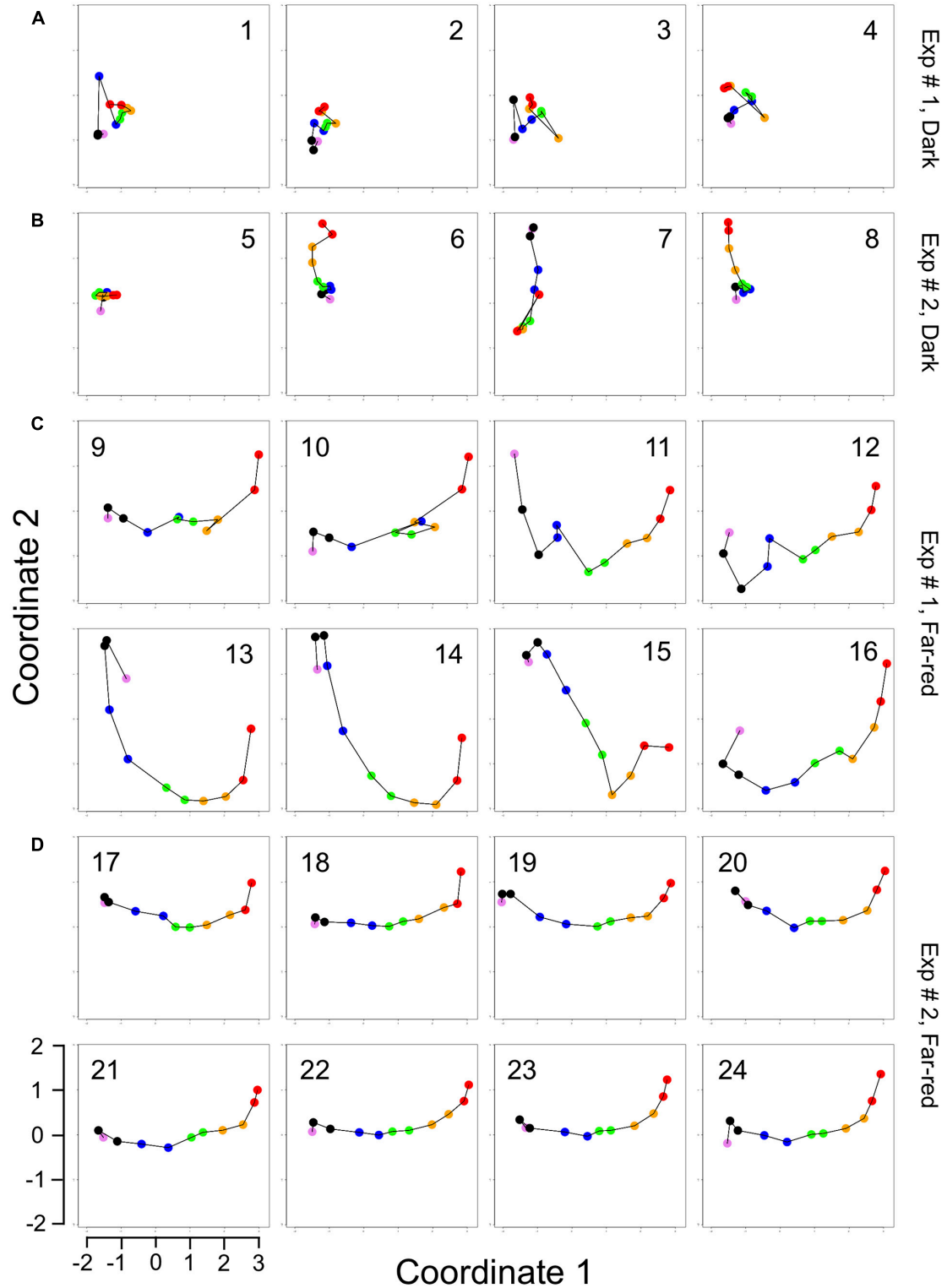


FIGURE 3 | Single cell trajectories of gene expression displayed after multidimensional scaling (MDS) of the expression patterns. Panels (A,B) show the trajectories of unstimulated cells of experiment #1 and experiment # 2, respectively. Panels (C,D) show the trajectories of far-red stimulated cells of the two experiments. Each data point represents the gene expression pattern of a cell at a given time point at 1 h time intervals. The start position (0 h) of each trajectory is encoded in pink and the endpoint (10 h) in red. The number displayed in each subpanel refers to the ID number of the plasmodial cell (P1 to P24) as listed in **Table 2**. All cells of the dark controls did not sporulate while all far-red irradiated cells sporulated. All plots are displayed at the same scale.

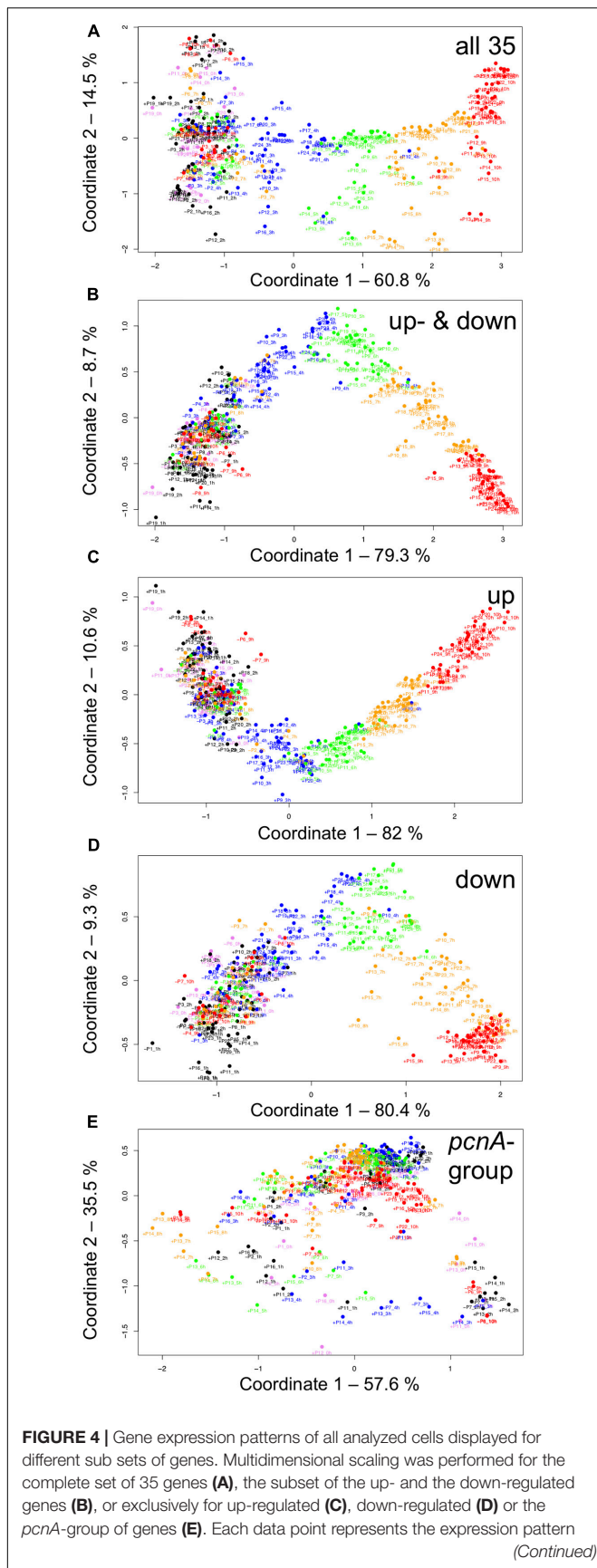


FIGURE 4 | Continued of an individual cell at a given time point. Time is encoded by color (0 h, pink; 1 h, 2 h, black; 3 h, 4 h, blue; 5 h, 6 h, green; 7 h, 8 h, ochre; 9 h, 10 h, red). Developmental destiny, cell number (as assigned in Table 2), and time is given for each data point. The label + P12_1 h, for example, indicates that the data point refers to the expression pattern of plasmodium number 12 as measured at 1 h after the start of the experiment (corresponding to the onset of the far-red light stimulus in light-stimulated cells) and that the plasmodium had sporulated (+) in response to the stimulus (+, sporulated; -, not sporulated). The percent of variance is given for each coordinate.

Markov chain of states the cells assume in the course of their developmental trajectory and accordingly on their walk through the Waddington landscape. We assume that the Petri net represents the corresponding region of the Waddington landscape predicting possible developmental paths a single cell can follow, which of course yields a state machine.

Representing Markov chains as Petri nets comes with a couple of advantages.

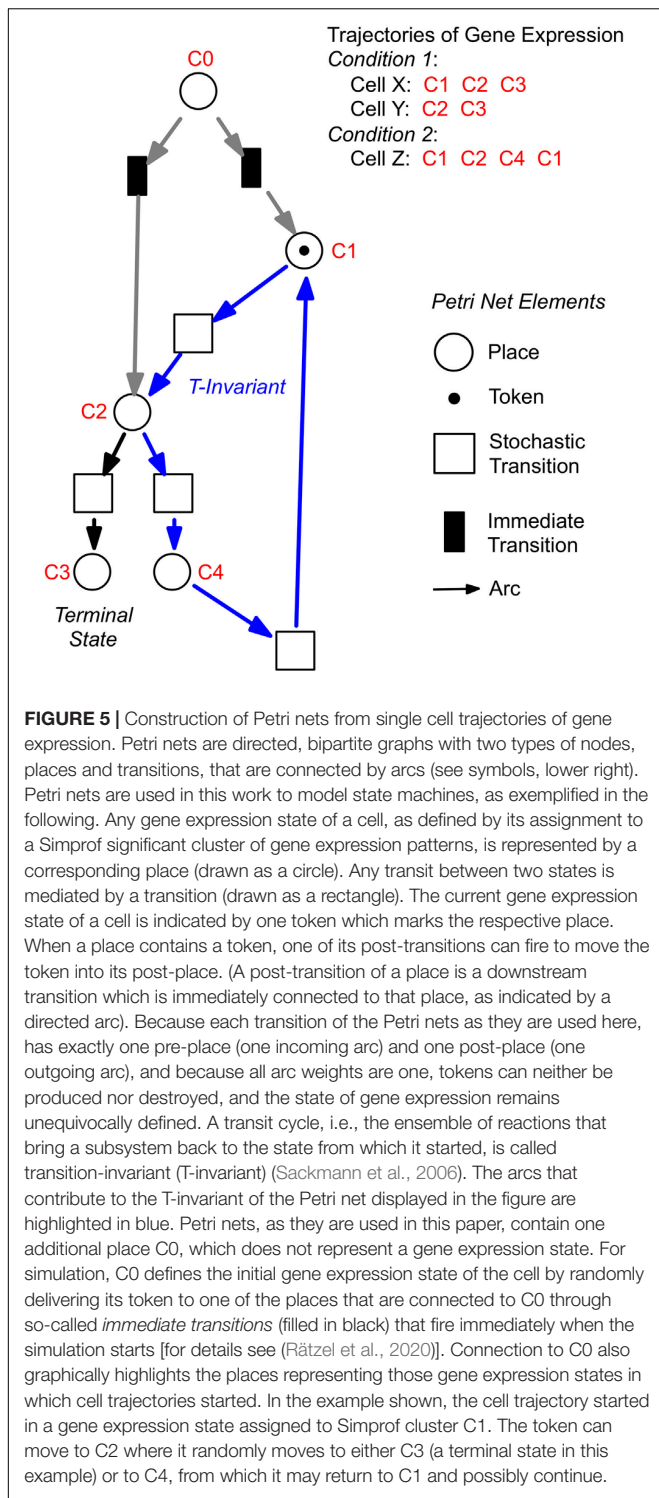
First, Petri nets are equipped with the concept of T-invariants, which belong to the standard body of Petri net theory from very early on (Lautenbach, 1973). We consider T-invariants as crucial in terms of biological interpretation of the generated net structures (Sackmann et al., 2006; Heiner, 2009). The computation of T-invariants is rather straightforward for state machines; due to their simple structure it holds:

- each cycle in a state machine defines a T-invariant, and
- each elementary cycle (no repetition of transitions) is a minimal T-invariant.

Second, modeling the differentiation-inducing stimuli, what we have not done so far, would turn some of the free choice conflicts into non-free choice conflicts, which involves, technically speaking, leaving the state machine net class. To unequivocally identify transits that are stimulus-dependent, we need a higher data density which we will hopefully achieve in one of our next experiments. With stimulus-dependent transitions, the constructed Petri nets and their Markov chains do not coincide anymore, instead the Markov chains as well as the reachability graph are directly derived from the Petri nets and may be analyzed by standard algorithms. Finally, our Petri net approach paves the way for the actual ultimate goal of our future work - reconstructing the underlying gene regulatory networks based on the reachability graphs encoded by the Waddington landscape Petri nets.

Characterization of Petri Nets Constructed From Gene Expression Data

Figure 6 displays a Petri net assembled from cell trajectories considering the set of 35 genes. The graphical representation laid out using the Sugiyama algorithm emphasizes the directionality of concurrent processes (Sugiyama et al., 1981). The net indicates that cells started in different states (connected to C0; see Legend to Figure 5 for details) and, after stimulation by far-red light, proceeded to a small set of terminal states (places C71, C76,



differently. Each place is colored according to the relative frequency of its corresponding gene expression state, indicating that some states occurred more frequently than others. From this representation it is obvious that cells of experiments #1 and #2 form different branches, in part projecting onto different terminal states, reflecting accordingly different developmental trajectories to commitment and sporulation. **Figure 6B** displays the same Petri net, but with a different color coding. Here, transitions are colored according to how frequent the corresponding transits occurred, indicating that some paths were more frequently taken than others. Places are colored according to their relative stability, defined as the average residence time of a cell in the respective state (see Methods for details). Coloring indicates that cells reached a terminal state through states of different stability, e.g., meta-stable intermediates.

Un-stimulated cells (**Table 2**, dark controls) spontaneously switched between significantly different states of gene expression. Their trajectories gave three disconnected Petri nets (**Figure 7A**; the three nets were connected to C0 for technical reasons, see legend to **Figure 5**).

Petri nets of **Figures 6A,B, 7A** indicate that the expression pattern in both, stimulated and un-stimulated cells developed predominantly in forward directions while there were some transits back to previous states creating so-called transition-invariants (T-Invariants; **Figure 5**). We asked whether stimulus-independent temporal expression differences like those observed in the subset of the *pcnA*-group of genes might have added to this directedness. Therefore, we constructed a Petri net from trajectories based on significant clusters, this time exclusively clustering the subset of up- and down-regulated genes. Basic features found in the Petri nets of up- and down-regulated genes were similar to the ones found in the Petri nets for the full set of 35 genes: Trajectories formed parallel main branches, there were intermediate nodes of different stability, of different connectedness, and hence states that occurred with different frequency (**Supplementary Figure 6**). In contrast, there was a high number of minimal T-invariants that heavily involved places representing gene expression states that occurred in un-stimulated cells. A Petri net built by considering only transits that occurred in un-stimulated cells (**Figure 7B**) was nearly covered with T-Invariants, indicating spontaneous, reversible alterations in the expression of up- and/or down-regulated genes. Again, states of gene expression displayed different stability. Considerable variation in the expression level of the up-and down-regulated genes is even most obvious from the heat map of initial states from which trajectories emerged and of terminal states that were observed during the experiment (**Figure 8**). The high density of T-invariants in the un-stimulated cells suggests that similarly, the T-invariants involving places corresponding to light-stimulated cells are due to gene expression changes that do spontaneously occur before cells are caught by a new attractor formed in response to the far-red stimulus (see Discussion).

Figure 7 also shows that selecting sets or subsets of genes for hierarchical clustering and subsequent Petri net construction may yield Petri nets of different structure delivering accordingly non-redundant information on corresponding subsets. This is also shown in **Table 4** for the set of 35 genes and for subsets, the

C77, C78, C79, C95) via multiple, more or less highly connected intermediate states. To facilitate the interpretation of the Petri net, we have colored the places and transitions according to different criteria. In **Figure 6A**, the transitions being specific to cells of experiments #1 or #2 and for dark controls or light-stimulated cells in the respective experiments, are colored

down-regulated, up-regulated, down- and up-regulated, and the *pcnA*-group of genes. Except for the *pcnA*-group, the number of places per gene was approximately the same. The number of transitions per gene however became less with more genes considered. This suggests that up-regulation, down-regulation and even expression of the *pcnA*-group of genes are at least partly coordinated or co-regulated processes. The average number of minimal T-invariants per gene compared for the different groups of genes (Table 4) suggests that reversibility observed for the subsets vanishes when more genes are considered, obviously due to combinatorial effects.

Single Cell Trajectories Reveal Qualitatively Different Patterns in Differential Gene Regulation

We have argued that Petri net modeling disentangles the complex response of cell reprogramming (Rätzel et al., 2020) and predicts feasible developmental pathways through the Waddington landscape, resulting in significantly distinct single cell trajectories. To reveal similarities and differences of the expression kinetics of individual genes, we plot the geometric mean of the concentration values of the mRNA in a cluster

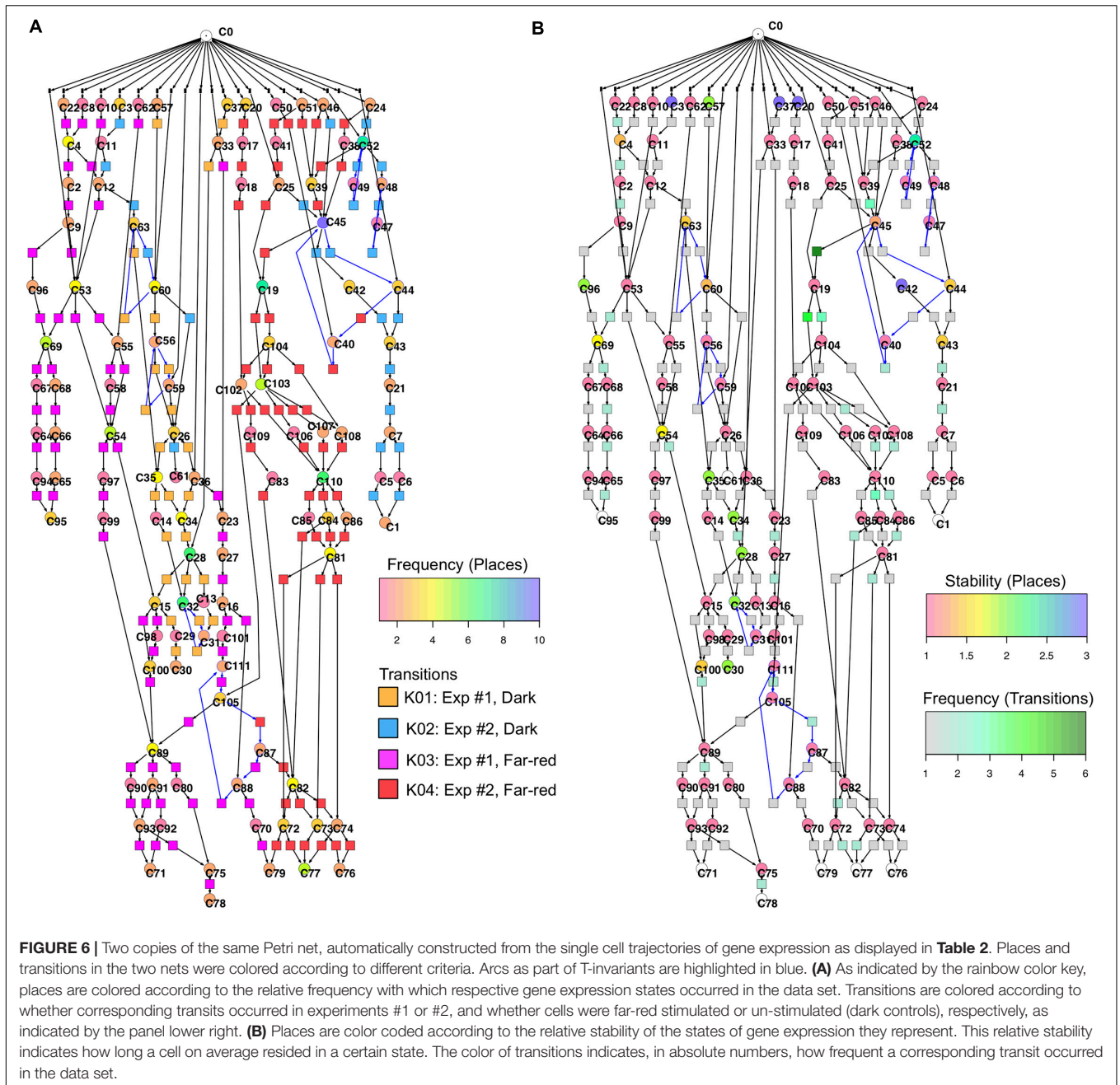
TABLE 2 | Single cell trajectories of gene expression.

Experiment	Cell	0.0 h	1.0 h	2.0 h	3.0 h	4.0 h	5.0 h	6.0 h	7.0 h	8.0 h	9.0 h	10.0 h
Exp #1, Dark	P1	60	56	59	26	35	34	34	28	28	32	31
Exp #1, Dark	P2	57	57	60	63	35	35	35	14	32	32	32
Exp #1, Dark	P3	59	56	26	36	34	34	28	13	31	32	32
Exp #1, Dark	P4	37	37	37	33	28	28	28	15	29	30	30
Exp #2, Dark	P5	24	52	52	52	49	52	52	52	48	47	48
Exp #2, Dark	P6	25	45	45	44	44	43	43	21	7	5	1
Exp #2, Dark	P7	3	3	3	11	12	63	63	60	60	26	61
Exp #2, Dark	P8	46	45	45	42	42	42	43	21	7	6	1
Exp #1, Far-red	P9	33	23	27	16	101	111	105	87	88	70	79
Exp #1, Far-red	P10	36	23	27	16	88	111	105	89	80	75	78
Exp #1, Far-red	P11	10	53	54	54	15	98	100	89	91	93	71
Exp #1, Far-red	P12	53	55	54	54	15	100	100	89	91	92	71
Exp #1, Far-red	P13	8	4	4	12	53	69	69	68	66	65	95
Exp #1, Far-red	P14	22	4	2	9	53	69	69	68	66	65	95
Exp #1, Far-red	P15	22	4	2	9	96	96	69	67	64	94	95
Exp #1, Far-red	P16	62	55	58	54	97	99	89	90	93	75	78
Exp #2, Far-red	P17	50	40	45	19	104	103	105	87	82	72	79
Exp #2, Far-red	P18	51	41	25	19	104	102	110	85	81	72	77
Exp #2, Far-red	P19	20	20	20	17	18	102	109	83	82	72	77
Exp #2, Far-red	P20	44	40	45	19	103	108	110	84	82	73	77
Exp #2, Far-red	P21	51	39	45	19	103	106	110	84	82	74	76
Exp #2, Far-red	P22	52	39	45	19	103	107	110	86	81	73	76
Exp #2, Far-red	P23	46	39	45	19	103	107	110	86	81	73	77
Exp #2, Far-red	P24	24	38	45	19	104	108	110	84	81	74	77

Trajectories are displayed as temporal sequences of gene expression states. Each state is given by the cluster ID number to which it was assigned by the Simprof algorithm. The two experiments, Exp #1 and Exp #2, were performed on two different days, respectively, with the same strain (LU897 × LU898) and under virtually identical experimental conditions. All cells of the dark controls did not sporulate while all far-red irradiated cells sporulated.

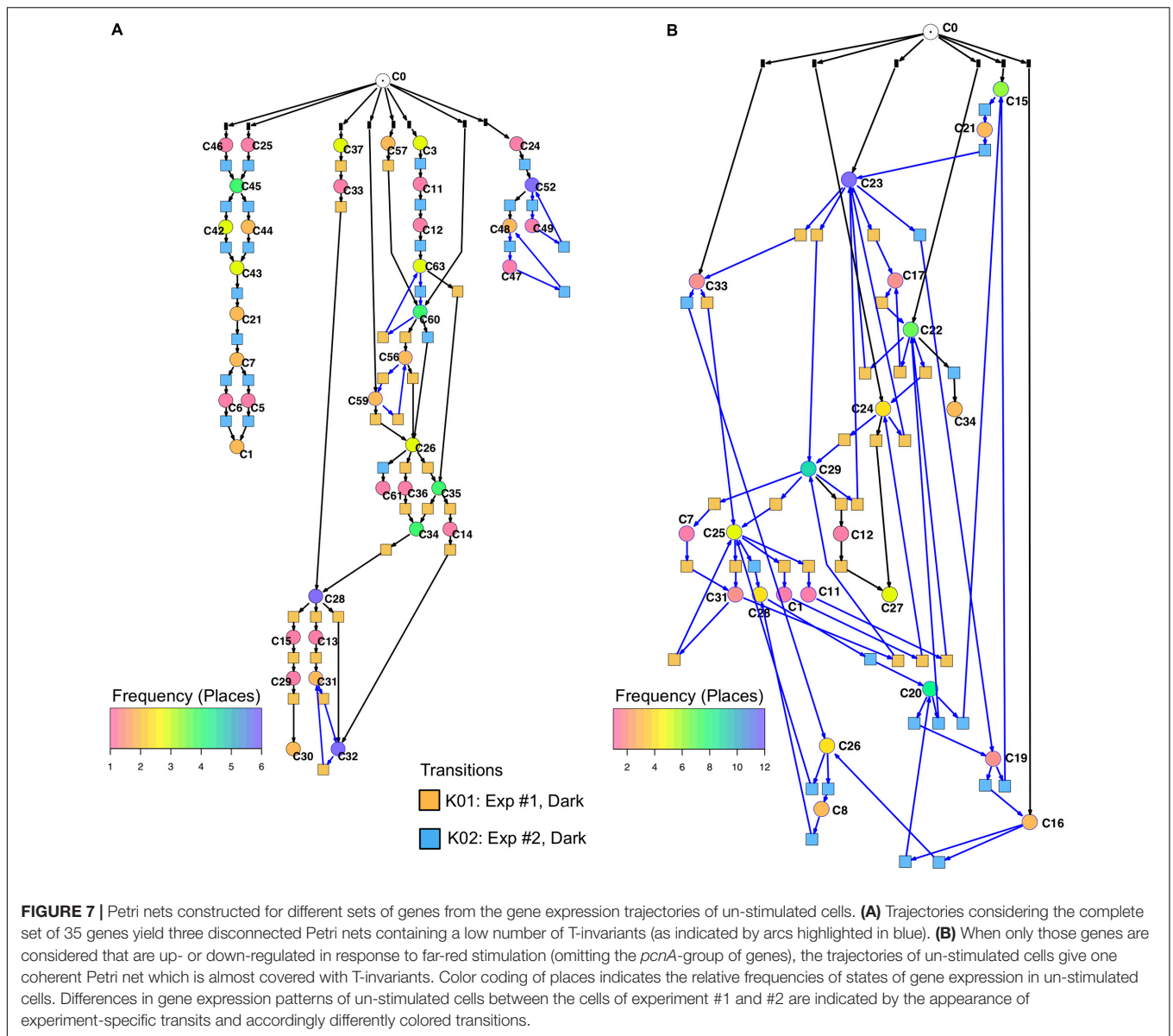
TABLE 3 | Terminology, basic modeling principles, and Petri net elements.

Place	Cellular state as defined by a significant cluster of gene expression patterns.
Transition	Transit, i.e., reprogramming step as defined by a discrete change in the state of gene expression.
Source place (no predecessor node)	The cellular state in which an experiment (recording of a time series) starts. There can be various source nodes, depending on the particular state in which a cell is in the moment when the experiment starts.
Sink node (no successor node)	Place with no outgoing arc, indicating a terminal state of gene expression reached at the end of the experiment. There can be multiple sink nodes.
Conflict	Forward branching places modeling bifurcation.
Token	The token indicates the cell and its current gene expression state; there is always just a single token.
Path	A single path from a source node to a sink node represents a possible developmental trajectory of a single cell. But a trajectory may not necessarily involve a source node and/or a sink node.
Petri net	The entire Petri net gives, for the genes analyzed, that part of the Waddington landscape through which cells passed and accordingly all corresponding developmental trajectories a single cell may undergo.



logarithmically, normalized to its concentration at the start of the experiment ($t = 0$ h) as a function of time for any single cell trajectory. In this kind of plot, the time course of the mRNA of each gene starts at the same point, while the slope of the curve indicates the x-fold change in mRNA abundance over time. Plotting subsets of genes suggests that trajectories through different regions of the Petri net of **Figure 6** indeed emerge from qualitatively different expression kinetics, and that genes are also differently regulated relative to each other when different trajectories are compared. In the example shown in **Figure 9**, *pldA* is early up-regulated in quite a number of trajectories, followed by *pwiA* and finally by *ligA* and *rgsA*

that appear strongly correlated at least in some of the plots. Qualitatively different patterns of regulation relative to each other are also evident for the three phospholipase D-encoding genes (**Supplementary Figure 7**). The *pldA* gene is up-regulated while *pldB* and *pldC* are down-regulated. In some of the trajectories, the initial change in the concentration of the *pldA* and *pldC* mRNAs is inverse as compared to the overall time course. A more comprehensive representation with more genes displayed makes similarities and differences between trajectories even more obvious (**Supplementary Figure 8**). Here, we observe a phenomenon, which is also seen in **Table 2**, namely that cells remain in a certain state for some time. This occurs



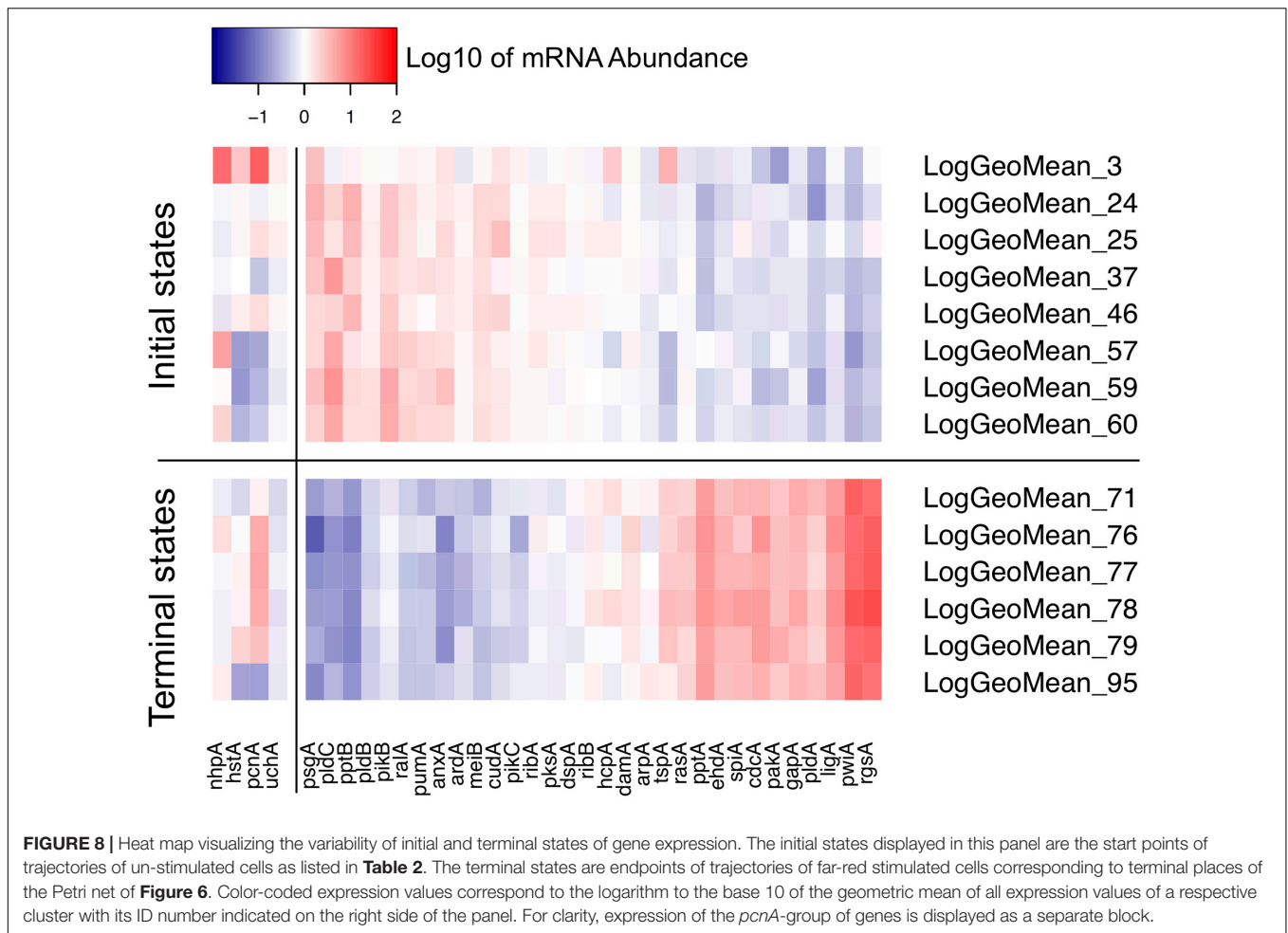
predominantly in the unstimulated cells but is also seen in some of the light stimulated cells, e.g., in those that proceed to state C95 (Figures 6A,B). Cells seemingly are trapped in a meta-stable state (e.g., C96, C69, C100, etc.; Figure 6B) for some time until the developmental program proceeds. We presumably will need more data to see whether this is an artifact which occurs by the discretization of gene expression through clustering. Conversely, discretization might help to identify tipping points for the differential regulation of gene expression as the plots in Supplementary Figure 8 suggest.

DISCUSSION

We have analyzed the gene expression dynamics in response to a differentiation-inducing stimulus pulse in true time by repeatedly

taking samples of large, multinucleate plasmodial cells. Control experiments have demonstrated that the gene expression patterns in samples simultaneously retrieved from different sites of a large plasmodial cell did not deviate within the range of the technical accuracy of the measurements. This again confirms that the plasmodial cytoplasm, at least at the level of macroscopic sampling, can be considered as a homogeneous reaction volume.

The injuries caused by multiple sampling of a plasmodial cell heal spontaneously and cutting the plasmodial mass neither induces nor prevents sporulation (Starostzik and Marwan, 1994, 1995b, 1998; Rätzel and Marwan, 2015). This is also confirmed for the large plasmodia used in this study through the dark controls that did not sporulate (Table 2 and Supplementary Figure 1), while the far-red light induced plasmodia sporulated. The changes in gene expression patterns observed in the dark controls seem to be spontaneous and not caused by repeated



sampling for the following reasons. First, plasmodia are in different states of gene expression already at the start of the experiments (**Figure 8** and **Table 2**), i.e., at the moment before the first sample is taken, so sampling cannot be the reason for this heterogeneity. Second, the trajectories of unstimulated cells developed in different directions although the sampling procedure was the same in all of these cells (**Figures 3A,B**), indicating that the shift in gene expression was not directed with respect to the start of the experiment. Third, the Petri net considering the differential regulation of the subset of light-regulated genes, the expression of which changed to some extent even in unstimulated cells, is almost completely covered with T-invariants (**Figure 7B**), indicating no directed change in the expression of this set of light-regulated genes, neither with respect to the start of the experiment nor with respect to the initial states in which the cells resided before the first sample was taken. We cannot exclude that certain genes might be differentially regulated in response to injury, e.g., genes involved in membrane biosynthesis, as leaks in the membrane readily heal. However, there seems to be no systematic effect on the differential expression of the genes analyzed in the present study.

In contrast to a typical mammalian cell, which has a relatively small cytoplasmic volume, while many genes are present in

two copies only, the plasmodial cell contains many millions of nuclei. These nuclei are suspended in a large cytoplasmic volume which continually mixes by the vigorous shuttle streaming. The T-invariants in the Petri nets of **Figure 7B** and **Supplementary Figure 6** indicating the up- and down-regulation of genes were due to changes in the mRNA concentration that occurred at distantly located sites of the plasmodium at the same time. Hence, it seems unlikely that these changes are stochastic gene expression noise. Instead, the T-invariants, presumably do reflect the (non-linear) dynamics of the system. Non-linear, switch-like behavior, bifurcations, multistability, or oscillations all certainly do have fundamental biological and functional implications, and the T-invariant analysis of true single cell time series can help to identify them.

Gene expression states of the cells were defined by hierarchical clustering and discretized by assigning each gene expression pattern to a Simprof significant cluster (Clarke et al., 2008; Rätzel et al., 2020). Trajectories of subsequent discrete states were then assembled into a state machine implemented as a Petri net. In the Petri net, each gene expression state is represented by a place and each transit between two states is represented by a transition.

The Petri net, as it has been defined in this and previous studies depends on the data pre-processing by clustering of the data

(Clarke et al., 2008; Werthmann and Marwan, 2017; Rätzel et al., 2020). It models gene expression trajectories as Markov chains (Gagniuc, 2017), which assumes that each subsequent state only depends on the current state of a cell and not on its previous states, i.e., it does not depend on the individual history of a cell. This assumption is commonly made by computing pseudo-time series from snapshots of individual mammalian cells (Bendall et al., 2014; Shin et al., 2015; Haghverdi et al., 2016; Marr et al., 2016; Street et al., 2018; Weinreb et al., 2018; Chen et al., 2019; Setty et al., 2019). It follows the principle of parsimony in making not more assumptions than necessary and giving the simplest possible explanation for an observed phenomenon. Practically this means that any path which a token can take through the Petri net, by stochastic firing of the transitions, translates into a feasible trajectory of an individual cell. Hence, firing of a transition does only depend on the marking of the pre-place of this transition and not on the identity of any upstream places from which the token originally came. Defining the cell's state of gene expression by measuring more genes might well diversify places and hence change the structure of the Petri net. This has been demonstrated by constructing nets from subsets of genes. In the examples provided, the structure of the Petri net changed and the number of T-invariants increased drastically upon reduction of the number of considered genes (Table 4).

If the structure of the Petri net does depend on the set of genes analyzed, what is its actual value? The actual value is that it reveals the behavior of states defined by sets or subsets of genes. Limiting the analysis to the chosen subset of up- and down-regulated genes, as we have done here, revealed extensive on- and off-switching of the genes in unstimulated cells that are differentially regulated in response to a differentiation-inducing stimulus. This became immediately obvious through structural analysis of the Petri net by determining the number of minimal T-invariants. Displaying the net in Sugiyama representation revealed another phenomenon with respect to this subset of genes. The light stimulus caused directed development toward a small number of terminal states reducing the overall number of alternative states in which the cells resided. This suggests that a cellular attractor is formed in response to the stimulus causing the commitment to differentiation.

Coloring the transitions of the Petri net according to the frequency by which transits occurred, allows identification and visualization of main paths, i.e., paths which the system preferably took. Coloring places according to the relative stability of the states they represent indicated metastable states that were not necessarily identical to highly connected places. Places having many pre-transitions (many incoming arcs) represent states, the system is likely to assume, like a corrie in the metaphor of the Waddington landscape, through which the system will pass. Places having many post-transitions (many out-going arcs) represent branching points from which the system has multiple options to proceed.

Our analysis has confirmed former observations (Rätzel et al., 2020), now at considerably larger resolution in time, that unstimulated cells spontaneously and reversibly change their expression pattern. These changes involved the expression of genes that are differentially regulated in response to a

differentiation-inducing stimulus. Spontaneous switching of gene expression patterns is at least one reason why stimulated cells started their way to commitment and differentiation from quite different states, indicating substantial heterogeneity in the population of cells. In other words, cells can start differentiation while being in various different states. The differentiation-inducing stimulus then collects or focusses these cells onto a narrow set of states like an attractor of a dynamic system would do. This phenomenon is graphically revealed by the funnel- or cone-like appearance of the Petri net in the Sugiyama layout (Supplementary Figure 6).

The response of a cell to a differentiation-inducing stimulus seems to depend on the cell's current internal state. Figure 6A revealed distinct main branches (visible through transitions of different color) for cells from experiment #1 as compared to experiment #2, suggesting that the response of the cell in terms of its developmental pathway did indeed depend on the initial physiological or gene expression state in which the cell resided while receiving the stimulus. The cells proceeded to slightly different terminal states that however might belong to the same cellular attractor.

One might be tempted to suspect a certain structure in the list of subsequently recorded trajectories (Table 2). Changes in the initial state of the plasmodia until the time of stimulus application might have occurred as the experiment proceeded. Similarities in subsequently recorded trajectories may be by chance and we cannot draw any final conclusion because the number of analyzed plasmodia is by far too low. With more plasmodia analyzed and more genes measured, we might discover that the individual history of a cell indeed matters, meaning that the Markov assumption is wrong. Even if this should be the case, the Petri net representation would still be valid, however with the firing probability of certain transitions depending on which path the token came from. Technically, this dependency could be implemented in the form of a colored Petri net. In this context it is trivial and at the same time

TABLE 4 | Number and relative frequency of places, transitions, and T-invariants of Petri nets constructed for different subsets of genes (see legend to Supplementary Figure 4) from the data of cells listed in Table 2.

Gene set	Down	Up	Up and down	All 35	<i>pcnA</i> etc.
Genes	10	10	20	35	4
Places	35	44	69	111	24
Transitions	105	114	144	159	59
P/Gene	3.5	4.4	3.5	3.2	6.0
T/Gene	10.5	11.4	7.2	4.5	14.8
Time points	11	11	11	11	11
Cells	24	24	24	24	24
P/(Genes × tps × cells)	0.013	0.017	0.013	0.012	0.023
T/(Genes × tps × cells)	0.040	0.043	0.027	0.017	0.056
T/P	3.00	2.59	2.09	1.43	2.46
T-Inv	4,413	1,371	1,063	7	732
T-Inv/Gene	441	137	53	0.20	183

P, places; *T*, transitions; *tps*, time points; *T-Inv*, T-invariants.

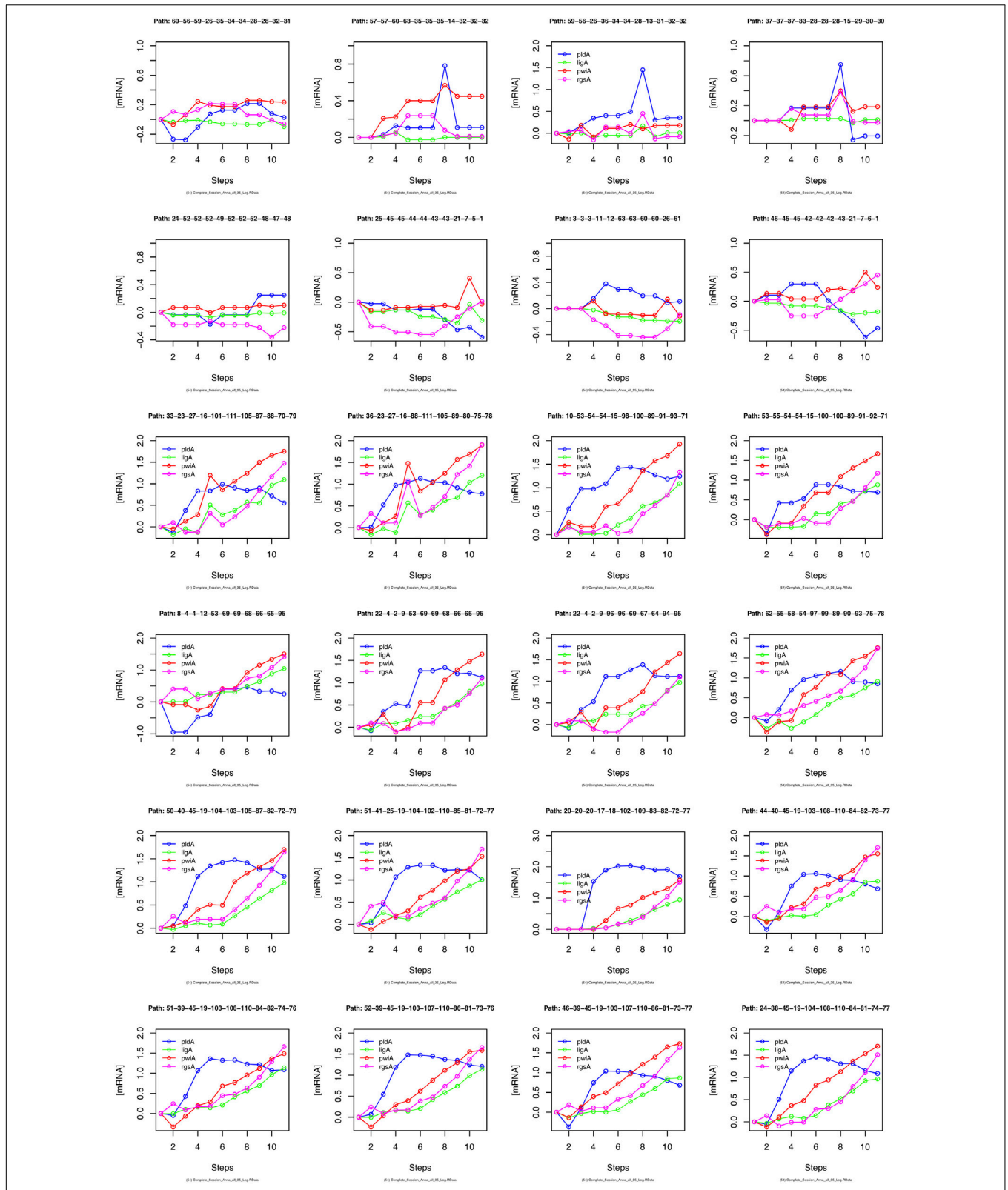


FIGURE 9 | Gene expression kinetics as derived from single cell trajectories. Each panel represents the trajectory of one single cell as characterized by subsequent states of expression of the same, arbitrarily chosen set of genes. For each gene, the logarithm to the base 10 of the geometric mean of the expression values of each cluster was plotted against time. Plotting the geometric mean instead of individual expression values results in discretization of the data while comparing different trajectories.

important to note that the identity of a place (i.e., state) is always defined by the set of genes that have been measured. Measuring more genes might split any place into more places or even into a separate Petri net with an increased overall number of places. This holds not only for states defined by gene expression but also for cellular states defined by the covalent modification of proteins, *etc.*

We have previously argued that the Petri net depicts aspects of the topology of the Waddington landscape (Waddington, 1957; Huang et al., 2009) with respect to and limited to the set of observed genes (or measured molecular entities) (Werthmann and Marwan, 2017; Rätzel et al., 2020). Then, the token in the Petri net corresponds to the marble rolling down the Waddington landscape as developmental processes unfold. Each Petri net place represents, albeit implicitly, a significantly distinct gene expression state. Despite this implicit representation, the temporal information on each gene for each cell trajectory is available and we have used this information to reveal the temporal hierarchy of differentially regulated genes. The Petri net representation disentangles accordingly the complex gene expression response and identifies alternative regulatory programs or routes. Using this information, the underlying regulatory network can be inferred by applying appropriate algorithms (Marwan et al., 2008; Durzinsky et al., 2011, 2013). This is a possible next step to go.

REFERENCES

- Alexopoulos, C. J., and Mims, C. W. (1979). *Introductory Mycology*, 3rd Edn. New York, NY: John Wiley Sons.
- Aselmeyer, F. (2019). *Analyse des Genexpressionsmusters an unterschiedlichen Stellen von Plasmodien von Physarum polycephalum (II)*. Bachelor Thesis Magdeburg: Otto von Guericke Universität.
- Bendall, S. C., Davis, K. L., Amir, E.-A. D., Tadmor, M. D., Simonds, E. F., Chen, T. J., et al. (2014). Single-cell trajectory detection uncovers progression and regulatory coordination in human B cell development. *Cell* 157, 714–725. doi: 10.1016/j.cell.2014.04.005
- Bornholdt, S., and Kauffman, S. (2019). Ensembles, dynamics, and cell types: Revisiting the statistical mechanics perspective on cellular regulation. *J. Theor. Biol.* 467, 15–22. doi: 10.1016/j.jtbi.2019.01.036
- Cannoodt, R., Saelens, W., and Saeyns, Y. (2016). Computational methods for trajectory inference from single-cell transcriptomics. *Eur. J. Immunol.* 46, 2496–2506. doi: 10.1002/eji.201646347
- Chen, H., Albergante, L., Hsu, J. Y., Lareau, C. A., Lo Bosco, G., Guan, J., et al. (2019). Single-cell trajectories reconstruction, exploration and mapping of omics data with STREAM. *Nat. Comm.* 10:1903.
- Clarke, K., Somerfield, P., and Gorley, R. (2008). Testing of null hypotheses in exploratory community analyses: similarity profiles and biota-environment linkage. *J. Exp. Mar. Biol. Ecol.* 366, 56–69. doi: 10.1016/j.jembe.2008.07.009
- Dove, W. F., Dee, J., Hatano, S., Haugli, F. B., and Wohlfarth-Bottermann, K.-E. (eds) (1986). *The Molecular Biology of Physarum polycephalum*. New York, NY: Plenum Press.
- Driesch, J. (2019). *Analyse des Genexpressionsmusters an unterschiedlichen Stellen von Plasmodien von Physarum polycephalum (I)*. Bachelor Thesis, Magdeburg: Otto von Guericke Universität.
- Durzinsky, M., Marwan, W., and Wagler, A. (2013). Reconstruction of extended Petri nets from time-series data by using logical control functions. *J. Math. Biol.* 66, 203–223. doi: 10.1007/s00285-012-0511-3
- Durzinsky, M., Wagler, A., and Marwan, W. (2011). Reconstruction of extended Petri nets from time series data and its application to signal transduction and to gene regulatory networks. *BMC Syst. Biol.* 5:113. doi: 10.1186/1752-0509-5-113

DATA AVAILABILITY STATEMENT

The raw data supporting the conclusions of this article are provided as part of the **Supplementary Material**.

AUTHOR CONTRIBUTIONS

AP and SP performed single cell time-series experiments and gene expression analyses and evaluated their results. MHa supervised the experimental work and developed the sample preparation method together with SP. MHe essentially contributed the analysis of the graph-theoretical properties of Petri nets and wrote a corresponding section of the manuscript. WM conceived and supervised the study, performed computational analyses including the automated generation of the Petri nets and wrote the manuscript. All authors read and approved the final version of the manuscript.

SUPPLEMENTARY MATERIAL

The Supplementary Material for this article can be found online at: <https://www.frontiersin.org/articles/10.3389/fgene.2020.612256/full#supplementary-material>

- Ferrell, J. E. Jr. (2012). Bistability, bifurcations, and Waddington's epigenetic landscape. *Curr. Biol.* 22, R458–R466.
- Gagnieu, P. A. (2017). *Markov Chains: From Theory to Implementation and Experimentation*. New York, NY: John Wiley & Sons.
- Gaublomme Jellert, T., Yosef, N., Lee, Y., Gertner Rona, S., Yang, Li, V., et al. (2015). Single-cell genomics unveils critical regulators of Th17 cell pathogenicity. *Cell* 163, 1400–1412. doi: 10.1016/j.cell.2015.11.009
- Glöckner, G., and Marwan, W. (2017). Transcriptome reprogramming during developmental switching in *Physarum polycephalum* involves extensive remodelling of intracellular signaling networks. *Sci. Rep.* 7:12304.
- Golderer, G., Werner, E. R., Leitner, S., Gröbner, P., and Werner-Felmayer, G. (2001). Nitric oxide synthase is induced in sporulation of *Physarum polycephalum*. *Genes Devel.* 15, 1299–1309. doi: 10.1101/gad.890501
- Gower, J. C. (1966). Some distance properties of latent root and vector methods used in multivariate analysis. *Biometrika* 53, 325–328. doi: 10.2307/2333639
- Graf, T., and Enver, T. (2009). Forcing cells to change lineages. *Nature* 462, 587–594. doi: 10.1038/nature08533
- Guttes, E., and Guttes, S. (1961). Synchronous mitosis in starved plasmodia of the myxomycete *Physarum polycephalum*. *Feder. Proc.* 20:419.
- Guttes, E., and Guttes, S. (1964). Mitotic synchrony in the plasmodia of *Physarum polycephalum* and mitotic synchronisation by coalescence of microplasmodia. *Meth. Cell Physiol.* 1, 43–54. doi: 10.1016/s0091-679x(08)62085-3
- Haghverdi, L., Büttner, M., Wolf, F. A., Büttner, F., and Theis, F. J. (2016). Diffusion pseudotime robustly reconstructs lineage branching. *Nat. Methods* 13:845. doi: 10.1038/nmeth.3971
- Hayashi, E., Aoyama, N., Wu, Y., Chi, H. C., Boyer, S. K., and Still, D. W. (2007). *Multiplexed, quantitative gene expression analysis for lettuce seed germination on GenomeLab™ GeXP genetic analysis system*. Beckman Coulter Application Information A-10295A. Available online at https://ls.beckmancoulter.co.jp/files/appli_note/A_10295A.pdf (accessed December 16, 2020).
- Heiner, M. (2009). “Understanding Network Behavior by Structured Representations of Transition Invariants,” in *Algorithmic Bioprocesses. Natural Computing Series*, eds A. Condon, D. Harel, J. Kok, A. Salomaa, and E. Winfree, (Berlin: Springer), 367–389. doi: 10.1007/978-3-540-88869-7_19
- Heiner, M., Rohr, C., and Schwarick, M. (2013). “MARCIE – Model Checking and Reachability Analysis Done Efficiently,” in *Application and Theory of Petri Nets*

- and Concurrency. *PETRI NETS 2013. Lecture Notes in Computer Science*, Vol. 7927, eds J. M. Colom, and J. Desel, (Berlin: Springer).
- Hoffmann, X.-K., Tesmer, J., Souquet, M., and Marwan, W. (2012). Futile attempts to differentiate provide molecular evidence for individual differences within a population of cells during cellular reprogramming. *FEMS Microbiol. Lett.* 329, 78–86. doi: 10.1111/j.1574-6968.2012.02506.x
- Huang, S., Ernberg, L., and Kauffman, S. (2009). Cancer attractors: a systems view of tumors from a gene network dynamics and developmental perspective. *Semin. Cell Dev. Biol.* 20, 869–876. doi: 10.1016/j.semcdb.2009.07.003
- Il Joo, J., Zhou, J. X., Huang, S., and Cho, K.-H. (2018). Determining relative dynamic stability of cell states using boolean network model. *Sci. Rep.* 8:12077.
- Junker, J. P., and van Oudenaarden, A. (2014). Every cell is special: Genome-wide studies add a new dimension to single-cell biology. *Cell* 157, 8–11. doi: 10.1016/j.cell.2014.02.010
- Kafri, R., Levy, J., Ginzberg, M. B., Oh, S., Lahav, G., and Kirschner, M. W. (2013). Dynamics extracted from fixed cells reveal feedback linking cell growth to cell cycle. *Nature* 494, 1–4. doi: 10.1201/b14602-2
- Lamparter, T., and Marwan, W. (2001). Spectroscopic detection of a phytochrome-like photoreceptor in the myxomycete *Physarum polycephalum* and the kinetic mechanism for the photocontrol of sporulation by P_{pf}. *Photochem. Photobiol.* 73, 697–702. doi: 10.1562/0031-8655(2001)073<0697:sdoapl>2.0.co;2
- Lautenbach, K. (1973). Exact liveness conditions of a Petri net class. GMD Report 82, Bonn (in German).
- Macaulay, I. C., Svensson, V., Labalette, C., Ferreira, L., Hamey, F., Voet, T., et al. (2016). Single-cell RNA-sequencing reveals a continuous spectrum of differentiation in hematopoietic cells. *Cell Rep.* 14, 966–977. doi: 10.1016/j.celrep.2015.12.082
- Marco, E., Karp, R. L., Guo, G., Robson, P., Hart, A. H., Trippa, L., et al. (2014). Bifurcation analysis of single-cell gene expression data reveals epigenetic landscape. *Proc. Natl. Acad. Sci. U S A* 111, E5643–E5650.
- Marquardt, P., Werthmann, B., Raetzl, V., Haas, M., and Marwan, W. (2017). Quantifying 35 transcripts in a single tube: Model-based calibration of the GeXP RT-PCR assay. *bioRxiv*. doi: 10.1101/159723
- Marr, C., Zhou, J. X., and Huang, S. (2016). Single-cell gene expression profiling and cell state dynamics: collecting data, correlating data points and connecting the dots. *Curr. Opin. Biotechnol.* 39, 207–214. doi: 10.1016/j.copbio.2016.04.015
- Marwan, W., Wagler, A., and Weismantel, R. (2008). A mathematical approach to solve the network reconstruction problem. *Math. Meth. Oper. Res.* 67, 117–132. doi: 10.1007/s00186-007-0178-5
- Moignard, V., Woodhouse, S., Haghverdi, L., Lilly, A. J., Tanaka, Y., Wilkinson, A. C., et al. (2015). Decoding the regulatory network of early blood development from single-cell gene expression measurements. *Nat. Biotechnol.* 33, 269–276. doi: 10.1038/nbt.3154
- Moris, N., Pina, C., and Arias, A. M. (2016). Transition states and cell fate decisions in epigenetic landscapes. *Nat. Rev. Genet.* 7, 693–703. doi: 10.1038/nrg.2016.98
- Paul, F., Arkin, Ya, Giladi, A., Jaitin Diego, A., Kenigsberg, E., et al. (2015). Transcriptional heterogeneity and lineage commitment in myeloid progenitors. *Cell* 163, 1663–1677. doi: 10.1016/j.cell.2015.11.013
- Plass, M., Solana, J., Wolf, F. A., Ayoub, S., Misios, A., Glazár, P., et al. (2018). Cell type atlas and lineage tree of a whole complex animal by single-cell transcriptomics. *Science* 360:eaq1723. doi: 10.1126/science.aaq1723
- R Core Team. (2016). *R: A language and environment for statistical computing*. Vienna: R Foundation for Statistical Computing.
- Rätzl, V. (2015). *Dynamische Fließgleichgewichte und ihre Übergänge in Reaktionsnetzwerken: Experimenteller Nachweis der Quasi-potential-Landschaft der zellulären Reprogrammierung*. Magdeburg: Otto von Guericke University.
- Rätzl, V., and Marwan, W. (2015). Gene expression kinetics in individual plasmoidal cells reveal alternative programs of differential regulation during commitment and differentiation. *Dev. Growth Differ.* 57, 408–420. doi: 10.1111/dgd.12220
- Rätzl, V., Werthmann, B., Haas, M., Strube, J., and Marwan, W. (2020). Disentangling a complex response in cell reprogramming and probing the Waddington landscape by automatic construction of Petri nets. *BioSystems* 189:104092. doi: 10.1016/j.biosystems.2019.104092
- Rohr, C., Marwan, W., and Heiner, M. (2010). Snoopy—a unifying Petri net framework to investigate biomolecular networks. *Bioinformatics* 26, 974–975. doi: 10.1093/bioinformatics/btq050
- Rusch, H. P., Sachsenmaier, W., Behrens, K., and Gruter, V. (1966). Synchronization of mitosis by the fusion of the plasmodia of *Physarum polycephalum*. *J. Cell Biol.* 31, 204–209. doi: 10.1083/jcb.31.1.204
- Sackmann, A., Heiner, M., and Koch, I. (2006). Application of Petri net based analysis techniques to signal transduction pathways. *BMC Bioinform.* 7:482. doi: 10.1186/1471-2105-7-482
- Saelens, W., Cannoodt, R., Todorov, H., and Saeys, Y. (2019). A comparison of single-cell trajectory inference methods. *Nat. Biotechnol.* 37, 547–554. doi: 10.1038/s41587-019-0071-9
- Schaap, P., Barrantes, I., Minx, P., Sasaki, N., Anderson, R. W., Bénard, M., et al. (2016). The *Physarum polycephalum* genome reveals extensive use of prokaryotic two-component and metazoan-type tyrosine kinase signaling. *Genome Biol. Evol.* 8, 109–125. doi: 10.1093/gbe/evv237
- Setty, M., Kisieliovas, V., Levine, J., Gayoso, A., Mazutis, L., and Pe'er, D. (2019). Characterization of cell fate probabilities in single-cell data with Palantir. *Nat. Biotechnol.* 37, 451–460. doi: 10.1038/s41587-019-0068-4
- Shin, J., Berg, D. A., Zhu, Y., Shin, J. Y., Song, J., Bonaguidi, M. A., et al. (2015). Single-cell RNA-seq with Waterfall reveals molecular cascades underlying adult neurogenesis. *Stem Cell* 17, 360–372. doi: 10.1016/j.stem.2015.07.013
- Spiller, D. G., Wood, C. D., Rand, D. A., and White, M. R. H. (2010). Measurement of single-cell dynamics. *Nature* 465, 736–745.
- Starostzik, C., and Marwan, W. (1994). Time-resolved detection of three intracellular signals controlling photomorphogenesis in *Physarum polycephalum*. *J. Bacteriol.* 176, 5541–5543. doi: 10.1128/jb.176.17.5541-5543.1994
- Starostzik, C., and Marwan, W. (1995a). Functional mapping of the branched signal transduction pathway that controls sporulation in *Physarum polycephalum*. *Photochem. Photobiol.* 62, 930–933. doi: 10.1111/j.1751-1097.1995.tb09158.x
- Starostzik, C., and Marwan, W. (1995b). A photoreceptor with characteristics of phytochrome triggers sporulation in the true slime mould *Physarum polycephalum*. *FEBS Lett.* 370, 146–148. doi: 10.1016/0014-5793(95)00820-y
- Starostzik, C., and Marwan, W. (1998). Kinetic analysis of a signal transduction pathway by time-resolved somatic complementation of mutants. *J. Exp. Biol.* 201, 1991–1999.
- Street, K., Risso, D., Fletcher, R. B., Das, D., Ngai, J., Yosef, N., et al. (2018). Slingshot: cell lineage and pseudotime inference for single-cell transcriptomics. *BMC Genomics* 19:477. doi: 10.1186/s12864-018-4772-0
- Sugiyama, K., Tagawa, S., and Toda, M. (1981). Methods for visual understanding of hierarchical system structures. *IEEE Transac. Syst. Man Cyber.* 11, 109–125. doi: 10.1109/tsmc.1981.4308636
- Waddington, C. H. (1957). *The Strategy of the Genes; a Discussion of Some Aspects of Theoretical Biology*. London: Allen & Unwin.
- Walter, P., Hoffmann, X.-K., Ebeling, B., Haas, M., and Marwan, W. (2013). Switch-like reprogramming of gene expression after fusion of multinucleate plasmodial cells of two *Physarum polycephalum* sporulation mutants. *Biochem. Biophys. Res. Comm.* 435, 88–93. doi: 10.1016/j.bbrc.2013.04.043
- Warnes, G. R., Bolker, B., Bonebakker, L., Gentleman, R., Huber, W., Liaw, A., et al. (2016). *gplots: Various R Programming Tools for Plotting Data*. R package version 3.0.
- Weinreb, C., Wolock, S., Tusi, B. K., Socolovsky, M., and Klein, A. M. (2018). Fundamental limits on dynamic inference from single-cell snapshots. *Proc. Natl. Acad. Sci.* 115, E2467–E2476.
- Werthmann, B., and Marwan, W. (2017). Developmental switching in *Physarum polycephalum*: Petri net analysis of single cell trajectories of gene expression indicates responsiveness and genetic plasticity of the Waddington quasipotential landscape. *J. Phys. D Appl. Phys.* 50:464003. doi: 10.1088/1361-6463/aa8e2b
- Whitaker, D., and Christman, M. (2014). *clustsig: Significant Cluster Analysis*. R package version 1.1.
- Zhou, J. X., and Huang, S. (2011). Understanding gene circuits at cell-fate branch points for rational cell reprogramming. *Trends Genet.* 27, 55–62.

Conflict of Interest: The authors declare that the research was conducted in the absence of any commercial or financial relationships that could be construed as a potential conflict of interest.

Copyright © 2021 Pretschner, Pabel, Haas, Heiner and Marwan. This is an open-access article distributed under the terms of the Creative Commons Attribution License (CC BY). The use, distribution or reproduction in other forums is permitted, provided the original author(s) and the copyright owner(s) are credited and that the original publication in this journal is cited, in accordance with accepted academic practice. No use, distribution or reproduction is permitted which does not comply with these terms.